https://dx.doi.org/10.1016/j.jclepro.2020.125131
This is the Pre-Published Version.

Green Tunnel Pavement: Polyurethane Ultra-Thin Friction Course and its Performance Characterization

Bin Hong[1], Guoyang Lu[2,3], Junling Gao[1], Shuai Dong[1] and Dawei Wang[1,3,*]

[1] *School of Transportation Science and Engineering, Harbin Institute of Technology, Harbin 150090, P.R. China*

binhong@hit.edu.cn (B.H.); 18S132071@stu.hit.edu.cn (J.G.); 2273405697@qq.com (S.D.)

[2] *Department of Civil and Environmental Engineering, The Hong Kong Polytechnic University, 11 Yuk Choi Road, Hung Hom, Kowloon, Hong Kong*

guoyang.lu@polyu.edu.hk (G.L.)

[3] *Institute of Highway Engineering, RWTH Aachen University, Aachen 52074, Germany*

* Corresponding author.

Postal address: 73 Huanghe Road, Nangang District, Harbin 150090, P.R. China.

Email address: wang@isac.rwth-aachen.de

Tel.: +86-451-86282840

Fax: +86-451-86282116

© 2020. This manuscript version is made available under the CC-BY-NC-ND 4.0 license http://creativecommons.org/licenses/by-nc-nd/4.0/

Abstract: During the construction process of tunnel asphalt pavement, a lot of asphalt fume can be generated. The asphalt fume usually cannot dissipate quickly during the tunnel's construction, resulting in significant harm to the workers' health and extending traffic congestion. To solve the problem, a new tunnel pavement, polyurethane (PU) ultra-thin friction courses (PU/UTFC) was proposed, with excellent mechanical properties and wear resistance, and almost no harmful emissions due to its room temperature construction. For this purpose, two PU mixtures (PUM), PU-based open-graded friction courses (PU/OGFC) and PU concrete (PUC), with three different component ratios were investigated in terms of the mechanical properties, functional properties, environmental impact evaluation, and thermo-mechanical properties. Results have shown that PUM, compared to conventional asphalt mixtures, possesses excellent mechanical properties, functional properties, such as skid resistance, noise absorption performance and flame-retardant property, as well as sound environmental properties. Specifically, the increase in isocyanate index (*R*) can significantly enhance the mechanical properties and water resistance of PUM but will reduce its freeze-thawing resistance. In contrast to PU/OGFC, PUC has higher mechanical properties but lower water stability. The above two PU/UTFCs will resolve significant problems in asphalt pavement in the tunnel and possess a broader application prospect.

Keywords: Polyurethane, ultra-thin friction courses (UTFC), environmental impact evaluation, mechanical properties, functional properties

1 Introduction

Tunnels are recognized as one of the most energy- and material-intensive infrastructures of transportation engineering. Considering the complex and unique service environment of the tunnel, for instance semi-enclosed space structure, week lighting, heavy noise pollution, high probability of fire and accessible to accident etc., pavement plays a crucial role in traffic safety of the tunnel (Bonati et al., 2012, Qiu et al., 2019).

Conventionally, pavements commonly applied in tunnels are mainly concrete pavements and asphalt pavements. For a long time, cement concrete pavement (CCP) has been widely used in tunnels due to its long service life and better bearing capacity (Ueckermann et al., 2015, Sun et al., 2018). However, the long construction period, the high noise generated by tire-road interaction and the fast deterioration rate of the skid resistance, have become the biggest obstacle for further applying the CCP in the tunnel (Wang et al., 2015, Lu et al., 2020a). To achieve requirements of safety, comfort, and environmental friendliness for tunnel pavement, in recent years, asphalt pavement has become more and more popular, due to the easy maintenance and good driving comfort (Wang et al., 2015). However, conventional asphalt pavements also cause significant safety and environmental concerns in tunnels, such as rutting, fatigue failure and high air pollution during construction and maintenance. Especially, in the construction of tunnel asphalt pavement, a large amount of asphalt fume, exhaust gas and dust will be released. Apart from it, flame retardant of asphalt is weak, and the combustion-supporting effect of the asphalt will increase the risk of tunnel fires (Qun and Guo, 2005, Moretti et al., 2016, Qiu et al., 2019). Hence, the tunnel pavements should not only behave excellent road performance and durability, but also meet the environmental requirements during the construction (Zhao et al., 2010, Huang et al., 2015, Leng et al., 2019).

Based on the increasing demand for functional pavements, novel materials and technologies are being developed to improve the sustainability and functionality of pavement (Liu et al., 2018, Wang et al., 2019, Yang et al., 2020). The innovative polyurethane (PU) binder was developed for the maintenance of existing roads and constructing new roads in the previous research, which material exhibits a high mechanical and chemical durability to overcome the challenges of conventional pavement mixtures (Lu et al., 2019a, Lu et al., 2019b). The mechanical strength of PU mixture is formed based on the reaction of polyol and Polymeric Methylene Diphenyl Isocyanate (PMDI). During the reaction process, the 2 liquid components cure and become solid polyurethane, thereby proving the mechanical strength between the aggregates. The excellent

performance of PU indicates that the material provides a favorable combination of functionality and mechanical properties (Lu et al., 2020c, Lu et al., 2020d). A high resistance to deformation and fatigue of pavement mixtures based on PU are comprehensively validated based on in-situ experiments (Lu et al., 2020b).

Based on the excellent properties of PU binder, a number of functional and sustainable pavement materials have been developed. Among those materials, the most widely known is Poroelastic Road Surface (PERS). PERS is a novel type of pavement surface, which includes recycled tire rubber into low-noise pavements as aggregate (Wang et al., 2017a, Wang et al., 2017b). Based on the PU binder applied in the previous research, the tensile strength was improved significantly in cold temperatures (Li et al., 2019). The sound absorption coefficients of PERS have higher and wider peaks compared with conventional porous asphalt (PA). It proved the suitability of PERS for urban roads in cold regions and outlined the significant economic and social benefits. In recent years, the innovative polyurethane ultra-thin overlay (PU/UTFC) has been developed especially for meeting the requirements of tunnel pavements. Compared with conventional tunnel pavement materials, significant improvements were observed in mechanical and functional properties as well as the environmental performance. Based on the ignition tests in a previous study (Leng et al., 2019), PU/UTFC exhibited a better flame retardancy compared to asphalt mixture as well as a lower heat release rate (HRR). Particularly, the ignition time of PU is larger than that of asphalt mixture, indicating that PU is more difficult to ignite than asphalt.

Based on the previous study, the concept of PU/UTFC may be a feasible and effective way to enrich the innovative functions of tunnel pavement. In this paper, the research aims to further evaluate the fundamental properties of PU/UTFC when applied in the tunnel. Conventional asphalt mixtures (open graded friction course (OGFC) and asphalt concrete (AC)) were selected as references. Compared with conventional tunnel pavement materials, significant improvements were observed in both mechanical and functional properties, as well as environmental performance. This study provides a comprehensive analysis and applicability evaluation of PU/UTFC, which makes it possible to widely use the material in the fully or semi-enclosed space for the pavement. The research results also provides practical significance for the further optimization design of the PU based pavement mixtures.

2 Experimental materials and methods

2.1 Raw materials and sample preparation

2.1.1 Polyurethane binder

Two-component polyurethane (PU) resin was used as the binder of UTFC, which is designed as PU/UTFC. The polyol component (Elastopave® C 6551/202 C-A) and isocyanate component (ElastoCoast® C 6551 C-B) are both provided by BASF Polyurethane Specialities (China) Co., Ltd. In this study, three different mass ratios between the polyol and isocyanate (PU ratios) were considered and listed to be 100:80, 100:65 and 100:45, which are designed as PU-I, PU-II and PU-III with decreasing isocyanate index (*R*), respectively. The reaction mechanism of the PU binder is shown in Eq. (1). The PU binder consists of the hard segments and soft segments, which provide the strength and toughness of the PU binder (Hepburn, 1992), respectively. It is worth noting that the optimal PU ratio, in theory, is recommended to be 100:65 by the supplier. Small adjustments to the PU ratio are mainly to investigate the effects of the PU ratios, namely isocyanate index, on the performance of the PU mixtures and further find the PU ratio suitable for the PU mixtures.

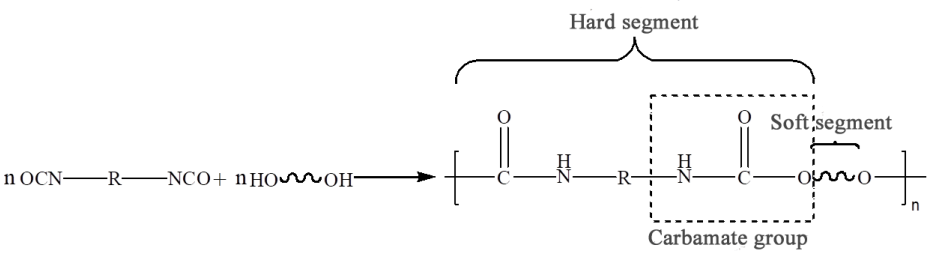

(1)

The basic performance, including tensile properties and viscoelastic properties, of the three PU binders were characterized. Both the specimens for the tensile test and viscoelastic test were prepared directly using the silicone rubber mould (seeing in Fig. 1a) with a cavity of the Type IV specimen size (Hong et al., 2018) described in ASTM D638-2010. Before preparation, the polyol component was dehydrated in a vacuum drying oven at 110 °C for 2 hours and cooled to the room temperature. The dehydrated polyol component and isocyanate component were weighed proportionally, and then mixed and stirred evenly by the glass rod at room temperature for about 2~3 minutes. Finally, the mixture was poured into the silicone rubber mould and then covered orderly by a Teflon film with 0.2 mm thickness, glass plate with 10 mm thickness and 5 Kg weight. The curing process was set at 25 °C for 24 hours. The formed tensile samples are shown in Fig. 1b. The viscoelastic samples were processed into 13 × 6 × 2 mm^3 from the tensile samples.

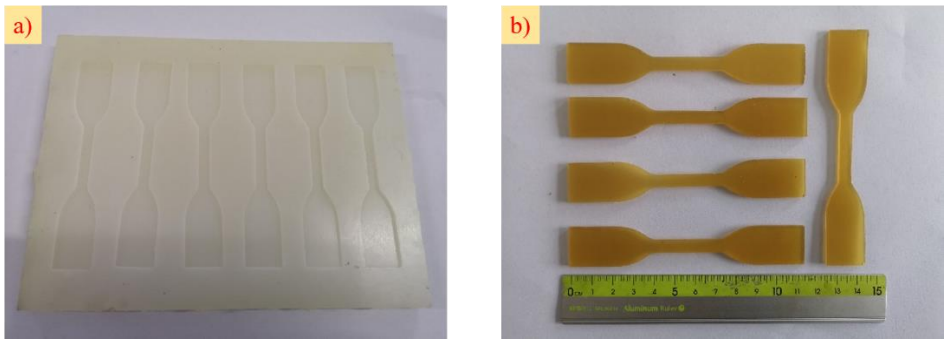

Fig. 1 The silicone rubber mould (a) and formed tensile samples (b)

2.1.2 PU mixtures

According to JTG F40-2004 (Technical Specification for Construction of Highway Asphalt Pavements) of China, two aggregate gradations, open-graded friction courses (OGFC-10) and asphalt concrete (AC-10) with the same nominal maximum sieve size, for PU/UTFC were chosen and shown in Table 1. It is noted that the PU mixtures (PUMs) with aggregate gradations of OGFC-10 and AC-10 were designed as PU/OGFC-10 and PU/AC-10 (or PUC-10), respectively.

Table 1 Mass percentage (%) passing the sieve size (mm) of OGFC-10 and AC-10, respectively

Type	Sieve size (mm)								
	13.2	9.5	4.75	2.36	1.18	0.6	0.3	0.15	0.075
OGFC-10	100	95	60	16	12	9.5	7.5	5.5	4
AC-10	100	95	60	44	32	22.5	16	11	6

Both PU/OGFC-10 and PU/AC-10 with a diameter of 101.6 mm ± 0.2 mm and height of 63.5 mm ± 0.2 mm (seeing in Fig. 2) were designed and prepared according to JTG F40-2004 for asphalt mixture. It should be noted that the pot-life of the PU mixtures is close to 1 hour at room temperature. It is exceedingly difficult for the current PU mixtures to control the material workability by using the conventional paving and compaction method for such a short pot-life. A new paving and compaction method or a new PU binder with enough long pot-life should be studied next. However, it does not prevent us from studying the application of PU mixtures in tunnel pavement.

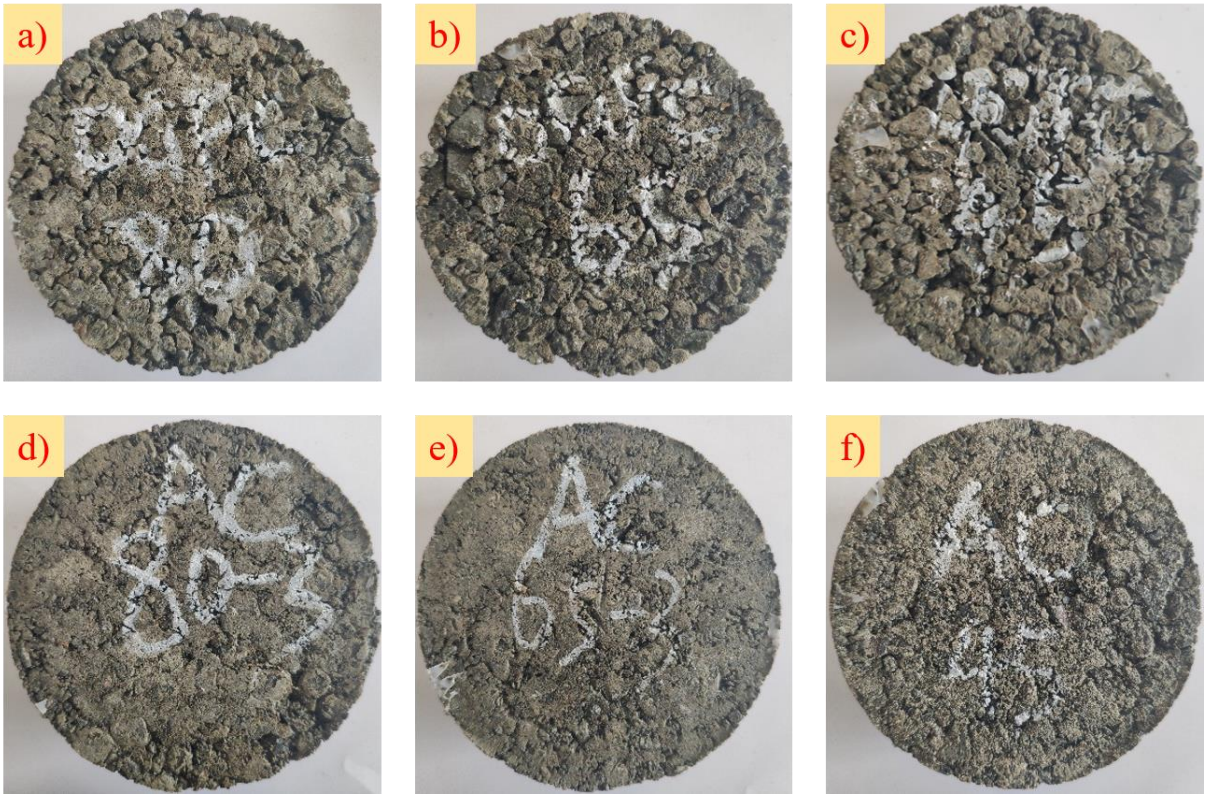

Fig. 2 PUMs: a) PU-I/OGFC-10, b) PU-II/OGFC-10, c) PU-III/OGFC-10, d) PU-I/AC-10, e) PU-II/AC-10, f) PU-III/AC-10

2.2 Material properties testing for the PU binder

2.2.1 Tensile properties

According to ASTM D638-2010, the tensile properties of the PU binder were tested at a load speed of 5 mm/min by using a universal mechanical testing machine (WDW-100E, Jinan, China). The size of specimens followed by the Type IV specimen with 33 mm length, 6 mm width, 2 mm thickness of the narrow section. Five effective parallel specimens were conducted and their average performance, including tensile strength, modulus and elongation at break, were calculated and analyzed.

2.2.2 Viscoelastic properties

The viscoelastic properties of the PU binder were characterized by both the temperature scanning and frequency scanning methods by using the dynamic shear rheometer (DSR, ARES-G2, TA, New Castle, America). The temperature scanning method was conducted under three-point bending mode at a frequency of 1 Hz, strain of 0.125% and heating rate of 3ºC/min from -50ºC to 90ºC. For this method, the loss factor

(tan δ), including the glass transition temperature (T_g) by tan δ and its peak height, and storage modulus as a function of temperature were analyzed and compared. The frequency scanning method was performed under three point bending mode at a strain of 0.125%.The temperature interval was set to 12°C from -36°C to 72°C under 15 Hz to 0.1 Hz of the frequency sweeping range. For this method, the complex modulus (G*) and phase angle (φ) as a function of frequency were analyzed in comparison.

2.2.3 Fourier transform infrared spectroscopy (FTIR) spectra analysis

The Fourier transform infrared spectroscopy (FTIR, AVATAR 360, Nicolet, Wisconsin State, USA) spectra of the three PU binders were obtained by the KBr disc technique from 4000 cm^{-1} to 450 cm^{-1}.

2.3 Material properties testing for PUMs

2.3.1 Volume parameters

According to JTG E20-2011 (Standard Test Methods of Bitumen and Bituminous Mixtures for Highway Engineering) (T 0705-2011) of China, the void ratio, voids in mineral aggregate (VMA) and bulk density of PUMs were tested and calculated. For each condition, five effective parallel samples were tested and the average value was obtained.

2.3.2 Cantabro loss

According to JTG E20-2011 (T 0733-2011), PUMs were immersed in water at 20 °C for 20 hours, and then take them out of the water and wipe the water off their surface using towel. After the above steps, the mass of each specimen was tested and recorded as m_0 with an accuracy of 0.1 g, and then all specimens were put into a Los Angeles testing machine and treated for 300 revolutions at 30 r/min. The mass of each residue sample was tested and recorded as m_1. When the residue sample is comminuted, the mass of the maximum sample will be recorded as m_1. For each condition, three effective parallel samples were tested. The Cantabro loss ($\triangle S$, %) was calculated by

$$\Delta S = \frac{m_0 - m_1}{m_0} \times 100 \quad (2)$$

The average of $\triangle S$ was obtained.

184 **2.3.3 Run-off loss**

185 With reference to JTG E20-2011 (T 0732-2011), the run-off loss of the two PUMs were conducted under
186 room temperature for 30 min since the PUM is stirred and cured at room temperature, and PU solidifies faster
187 at room temperature. The run-off loss can be calculated by

188 $$\Delta m = \frac{m_2 - m_0}{m_1 - m_0} \times 100 \quad (3)$$

189 where $\triangle m$ is the run-off loss (%) of PU, m_0 is the mass (g) of the beaker with a volume of 800 ml, m_1 is the
190 total mass of beaker and PUM for testing, m_2 is the total mass of beaker and residue PUM on its wall after
191 high-temperature treatment. For each condition, three effective parallel samples were tested and their average
192 was obtained.

193 **2.4 Mechanical properties testing for the PUMs**

194 **2.4.1 Marshall stability**

195 The Marshall stability (kN) of PUMs was tested according to JTG E20-2011 (T 0709-2011). It is noted
196 that an universal mechanical testing machine with a high measure range (250 kN) rather than the Marshall
197 tester was used in this test since the Marshall stability of PUMs has exceeded the range (100 kN) of the
198 Marshall tester. The loading rate was designed as 0.2 kN/s. In this study, standard Marshall stability and
199 immersed Marshall stability were evaluated accordingly after immersions in water for 30 min and 48 h at 60
200 ^{o}C. These two Marshall stabilities are designed as Marshall stability before and after water immersion,
201 respectively.

202 **2.4.2 Splitting strength**

203 Both the two splitting strengths of PUMs before and after freeze thawing were tested at 0.2 kN/s loading
204 rate and 25 ^{o}C testing temperature with concerning JTG E20-2011 (T 0729-2000). For the splitting strength
205 before freeze-thawing, the specimens were immersed in water for 2 h at 25 ^{o}C before testing. For the freeze-
206 thawing splitting strength, each specimen has frozen in a refrigerator for 16 h at -18 ^{o}C followed by immersing
207 in water for 24 h at 60 ^{o}C and then immersing also in water for 2 h at 25 ^{o}C before testing. For each condition,
208 four parallel samples were tested and the average value was obtained.

2.4.3 Trabecular bending

The trabecular bending properties of PUMs with size of 250 mm × 30 mm × 35 mm were tested at a loading rate of 5 mm/min and a testing temperature of 25 °C with reference to JTG E20-2011 (T 0715-2011). All specimens have been immersed in water for 45 min at 25 °C before testing. The flexural stress, maximum flexural strain and flexural stiffness modulus were calculated and evaluated. For each condition, five parallel samples were tested and the average value was calculated.

2.5 Functional properties testing for PUMs

2.5.1 Skid resistance performance

The skid resistance of the pavement surface plays a vital role in the traffic safety of the tunnel, which is characterized by the mean profile depth (MPD) and British pendulum number (BPN) using the self-made Laser texture scanner and British pendulum friction coefficient tester, respectively. The above tests were carried out after polishing every 30 minutes for 300 minutes using the self-made wheel accelerated polisher, Harbin Polishing Machine (HPM). The entire test process is shown in Fig. 3, in which HPM is shown in Fig. 3a.

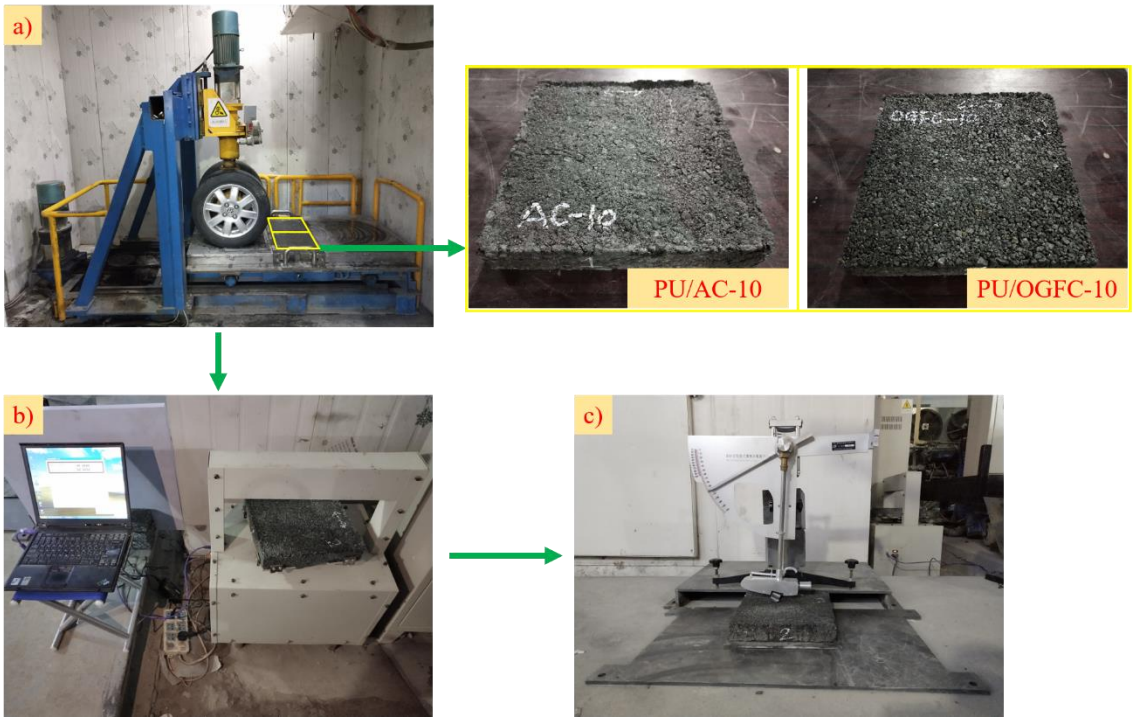

Fig. 3 The evaluation process of pavement skid resistance: a) Polishing; b) Mean profile depth (MPD) test; c) British pendulum number (BPN) test.

Detailed test processes are as follows:

1) Polishing: According to the preparation method of the rutting plate in JTG E20-2011 of China, the PUM specimens were prepared as a size of 30 cm × 30 cm × 5 cm. Before polishing, two samples were fixed in a self-made wheel accelerated polisher (seeing in Fig. 3a). The test parameters were designed as 1 kN of contact pressure between tire and sample, 10°C of room temperature, 4 times/min of the frequency of sample round-trip movement, 30 r/min of tire rotation speed, 15 ± 3 g/min of spraying speed of quartz sand (polishing agent) and 35 ± 5 mL/min of water spraying speed.

2) MPD test: After each 30 min of polishing, the MPD test with 0.2 mm of precision was conducted (seeing in Fig. 3b). The test parameters were designed as 142 mm of scanning radius and 5 mm of step size. Three effective parallel test points were tested and their average value was calculated.

3) BPN Test: After MPD testing, BPN was tested using the British pendulum friction coefficient tester (seeing in Fig. 3c). Five effective parallel test points were tested and their average value was calculated.

2.5.2 Acoustic performance

The acoustic performance of PUM samples with a cylindrical size of 40 mm × Φ100 mm was evaluated by the impedance tube method according to DIN EN ISO 10534-2. During the testing, the sound source and sound receiver are connected at the two ends of a tube, which can be seen in Fig. 4. The sample was fixed in the AFD 1000-AcoustiTube®. The sound source generated plane sound waves that penetrated the specimen, resulting in part of plane sound waves were absorbed and other plane sound waves were reflected. The absorbed and reflected acoustic pressures were measured by the wall-mounted microphones. The sound reflection factor, sound absorption factor and its impedance ratio (reflection factor/absorption factor) were calculated from the complex acoustic transfer functions of the two microphones using an analysis software "AFD 1001 - Determination of the sound absorption coefficient".

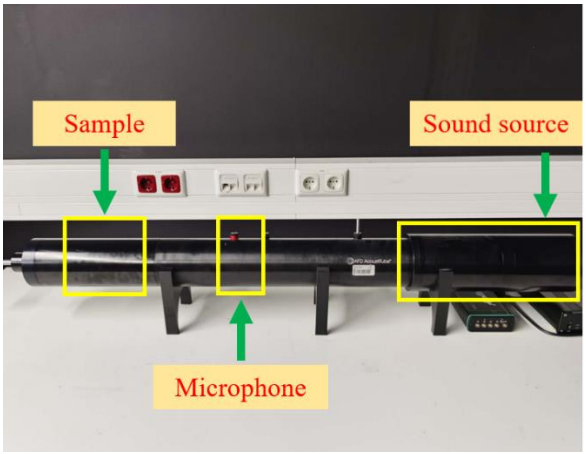

Fig. 4 The acoustic tube test

2.5.3 Flammability evaluation method

The combustion performance of both PU/OGFC and PU/AC with the three different PU ratios and size of 100 mm×100 mm×10 mm was evaluated by the cone calorimeter which consists of the carrier, combustion chamber, ventilation system, flue gas measuring system and gas analyzer (seeing in Fig. 5). Before testing, samples were wrapped with aluminum foil except for the top surface. The thermal radiation intensity and burning temperature were set to 50 kW/m^2 and 780°C, respectively, which is like the actual combustion environment. In this test, the heat release rate (HRR), total heat release (THR), effective combustion heat (EHC), ignition time (TTI), smoke and toxicity parameters, and mass change parameters (MLR) were measured to evaluate the combustion performance or flame retardancy of PUM.

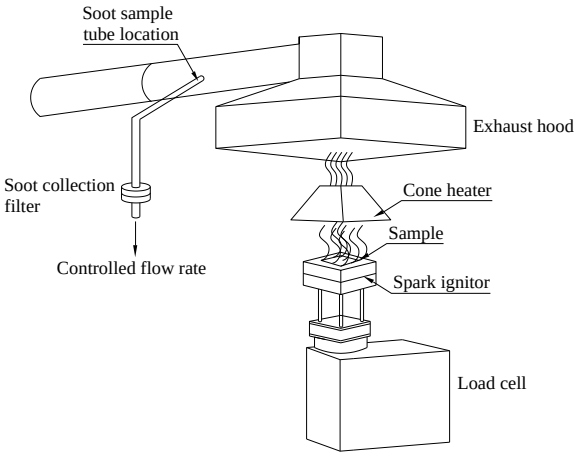

Fig. 5 The cone calorimeter

3 Environmental impact evaluation

It is reported that as much as 14% of global greenhouse gas (GHG) emissions is ascribed to the transport sector in which the construction, maintenance and usage of road alone account for 72% of these emissions pavement (Norman et al., 2006), making an important contributor to the anthropogenic burdening of the environment. To illustrate the advantage in pro-environment of the novel PUM when applied in tunnel pavement, the energy consumption and the GHG emissions of PUM during its construction process were analyzed (based on the existed standard frame of life cycle analysis (Santero et al., 2011, Harvey et al., 2016) by the comparison of asphalt mixtures. Their comparison results are plotted in Fig. 6.

In contrast to the heat requiring asphalt mixture, less energy for PUM is consumed during its construction stage based on room temperature manufacturing. Therefore, less GHG emissions existed in the construction of PUM. As shown in Fig. 6, both global warming potential (GWP) and energy consumption of the asphalt-based OGFC are significantly higher than that of PU/OGFC in the construction process.

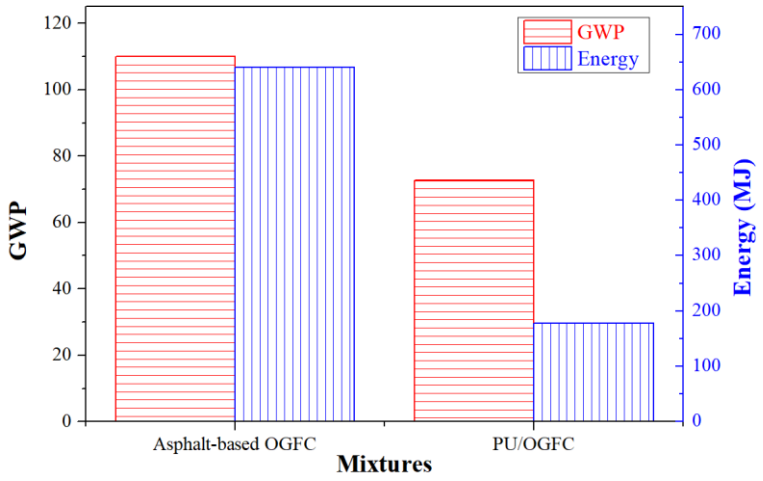

Fig. 6 Environmental impact analysis

Apart from it, it is also important that the whole life cycle is investigated as a substantial proportion of GHG emissions and energy consumption of PU mixtures during phases may also decrease, especially during the use phase. It is known that the amount of energy consumed and GHG emissions during the life cycle of a typical pavement highly depending on the traffic volume (Harvey et al., 2016). One can safely expect a better environmental performance of PUM in the congestion, usage and maintenance phases since there is a correlation between pavement structural strength and the number of times the asphalt needs replacement or maintenance. Also, a mechanical deficiency is linked to a rougher surface which increases the fuel

consumption of vehicles (Zhang et al., 2010). In general, the study indicates that PUM has more significant environmental benefits than asphalt throughout the life cycle stages which are, material production, transportation, construction and maintenance. Hence, it is a very suitable and sustainable material for the application in tunnel pavement.

4 Mix design of PUMs

As mentioned above, three different PU ratios (100:80, 100:65 and 100:45) were considered. To make sure that the aggregate gradation and the optimized PU content are consistent for both PU/OGFC-10 and PU/AC-10 mixtures with different PU compositions, the PU with 100:80 (Polyol to Isocyanate) was selected.

For the PU/OGFC-10 mixture, the Cantabro loss (<20%) and run-off loss (<0.3%) were utilized to determine the mass ratio between PU and aggregates (PU content) according to JTG F40-2004. The experimental results for both the Cantabro loss and run-off loss as a function of PU content with a range of 2%~6% are plotted in Fig. 7. As shown, the PU content should be not less than 3.5% to make that the Cantabro loss and run-off loss are less than 20% and 0.3%, respectively. For economic reasons, the PU content is determined as 4% for the PU/OGFC-10 mixtures with different PU ratios.

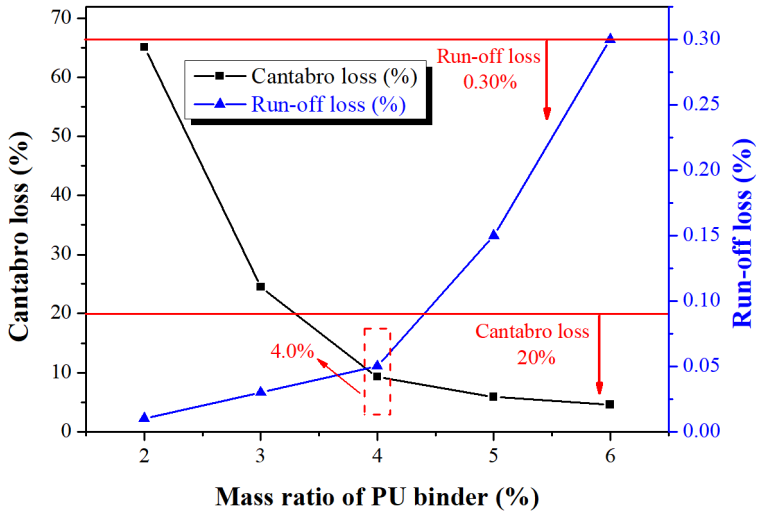

Fig. 7 Evolutions on the Cantabro loss and run-off loss for the PU/OGFC-10 mixtures

For the PU/AC-10 mixture, the optimized PU content is the content that makes the mixture achieve the highest Marshall stability and bulk density, but lowest void ratio and VMA at the same time according to JTG F40-2004. The above testing results are plotted in Fig. 8. As shown, the optimized PU content is 4.8% for the PU/AC-10 mixtures with different PU ratios.

Under the above mix parameters, the volume parameters of both PU/OGFC-10 and PU/AC-10 mixtures are listed in Table 2. As shown, both the PU/OGFC-10 and PU/AC-10 mixtures have similar volume parameters even under different PU ratios due to the same mix design. The relatively low void ratio for the PU-III/AC-10 mixture may be caused by an error during the preparation process.

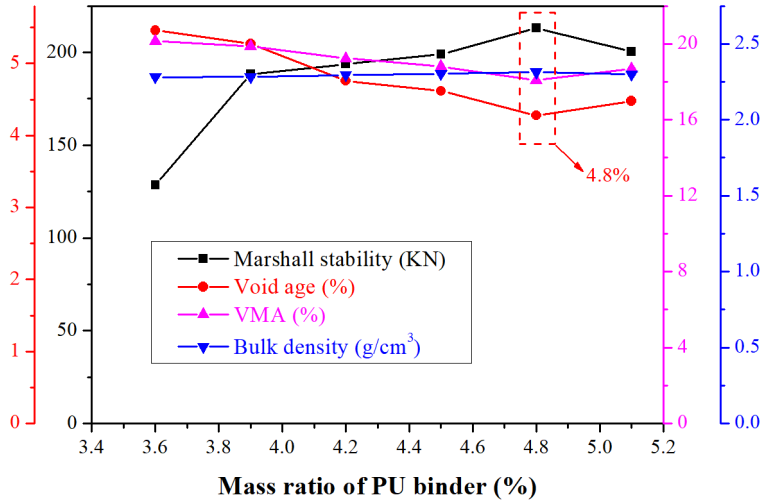

Fig. 8 Evolutions in the Marshall stability, bulk density, low void ratio and VMA for the PU/AC-10 mixtures

Table 2 The volume parameters of both PU/OGFC-10 and PU/AC-10 mixtures with different PU ratios

PUMs	PU binder	Bulk density	Void ratio	VMA
PU/OGFC-10	PU-I	2.03 ± 0.02	17.00 ± 0.76	26.90 ± 0.93
	PU-II	2.03 ± 0.02	17.06 ± 0.94	26.95 ± 0.81
	PU-III	2.04 ± 0.02	16.83 ± 0.79	26.76 ± 0.88
PU/AC-10	PU-I	2.30 ± 0.01	4.28 ± 0.44	18.09 ± 0.37
	PU-II	2.29 ± 0.02	4.56 ± 0.77	18.32 ± 0.66
	PU-III	2.33 ± 0.02	2.94 ± 0.67	16.93 ± 0.57

5 Results and discussion

5.1 Basic performance of the PU binders

5.1.1 Tensile properties

The tensile stress-strain curves of three PU binders are plotted in Fig. 9. As shown, an obvious and yield

phase exists in the tensile process of the PU-I binder while the yield phase gradually disappears with decreasing isocyanate index (*R*). The tensile properties of the three PU binders are listed in Table 3. As *R* decreases, the tensile strength and modulus of PU binder decrease notably while the elongation at break exhibits an opposite trend due to the increase in the soft segment. Accordingly, the toughness of the PU binder increases with decreasing *R*.

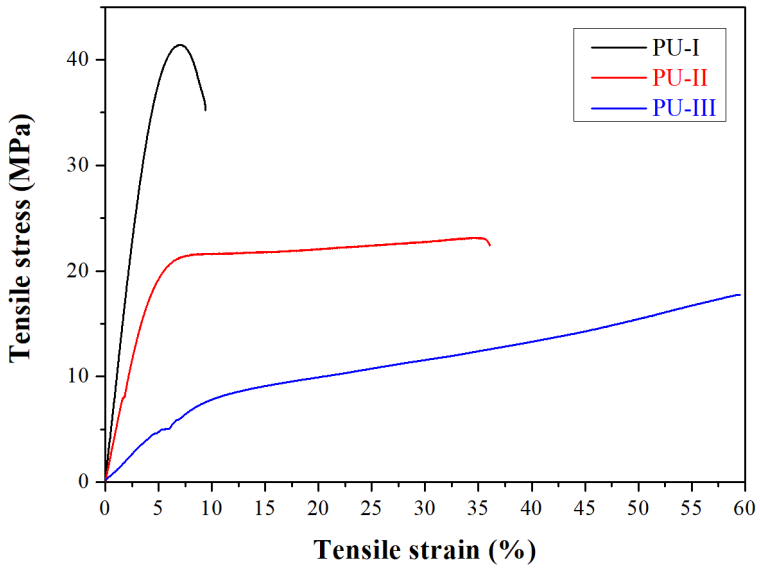

Fig. 9 The tensile stress-strain curves of the three PU binders

Table 3 Basic performance of the three PU binders

PU binders		PU-I	PU-II	PU-III
Tensile properties	Tensile strength (MPa)	42.30 ± 2.26	23.32 ± 0.85	17.84 ± 1.89
	Tensile modulus (MPa)	942.11 ± 43.92	482.17 ± 38.96	99.13 ± 5.50
	Elongation at break point (%)	9.43 ± 2.31	35.26 ± 1.60	57.25 ± 8.46
	T_g (°C)	60.0	43.2	44.1

5.1.2 Viscoelasticity properties

The development of loss factor (tan δ) and storage modulus in terms of temperature are plotted in Fig. 10 and Fig. 11, respectively. The glass transition temperatures (T_gs) by tan δ of the three PU binders are also listed in Table 3. Unlike the tensile strength and modulus, both T_g and storage modulus of the PU binder rapidly decreases and then recovers with increasing *R*, especially for the storage modulus with the highest

values at low temperatures. The average inter-crosslink molecular weight, M_c (g/mol), can be calculated by (Karbhari, 2006):

$$M_c = \frac{3RT\rho}{E_M} \quad (4)$$

where R is the universal gas constant (8.314J·mol^{-1}·K^{-1}), E_M is the storage modulus (MPa) of polymer in rubber state, ρ is the density of polymer (ρ is 1.20 g/cm^3 for all the three PU binders), T is the temperature at E_M. To make sure E_M is the storage modulus polymer in rubber state, T is equal to T_g + 30ºC. According to Eq. (4), M_cs of the PU binders are determined as 2179.9 g/mol, 2134.9 g/mol and 1701.5 g/mol as the decrease in R, respectively. It is also responsible for the reduction in tensile strength and modulus of the PU binder with increasing R.

Contrary to the tensile strength and modulus, the abnormal increase in both T_g and storage modulus below 10ºC for the PU-III may be due to excess polyols forming much more network of molecular chains (seeing in Eq. (1)) and strong hydrogen bonds (Hong and Xian, 2018) with isocyanates. Both the formation of more network of molecular chains and strong hydrogen bonds can improve the rigidity of molecular chains and further enhance the T_g and storage modulus at low temperature. However, the above enhancements do not improve the length of the hard segment that determines the tensile strength and modulus of PU, seeing in Eq. (1). The length of the hard segment is mainly determined by R, resulting in the tensile strength and modulus of PU decreases with increasing PU ratio.

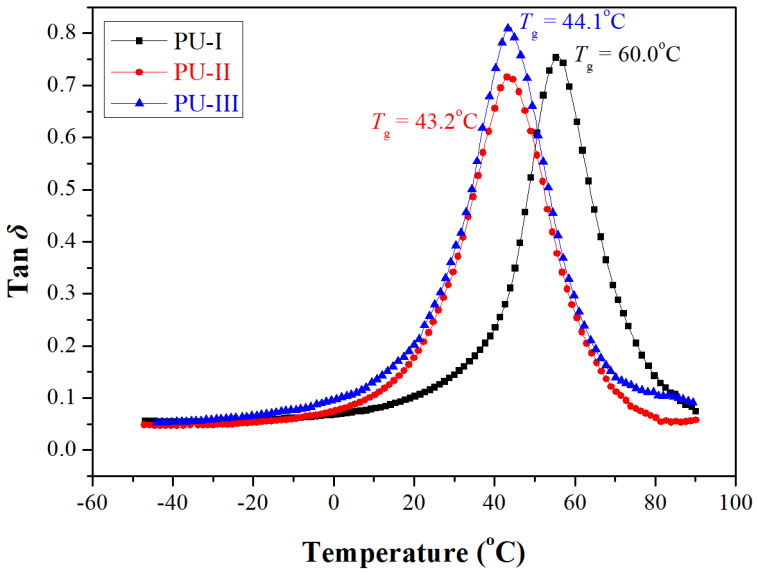

Fig. 10 Evolutions in tan δ of the PU binders as a function of temperature

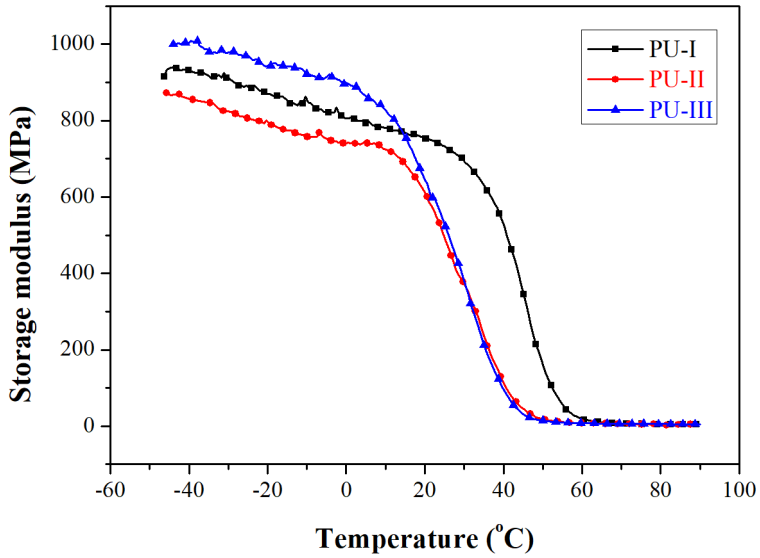

Fig. 11 Evolutions in storage modulus of the PU binders as a function of temperature

The complex modulus (G*) and phase angle (φ) as a function of frequency at the reference temperature of 36°C are plotted in Fig. 12 and Fig. 13, respectively. As shown in Fig. 12, as the decrease in *R*, G* decreases at a fast rate and then fairly slow rate in the low-frequency region, respectively, and increases slightly in the high-frequency region. This result has indicated that the PU binder becomes soft obviously and hardened slightly as the decrease in *R* in the low-frequency and high-frequency region, namely high-temperature and low-high-temperature region, respectively. However, the above changes become less obvious in the low *R*-value range.

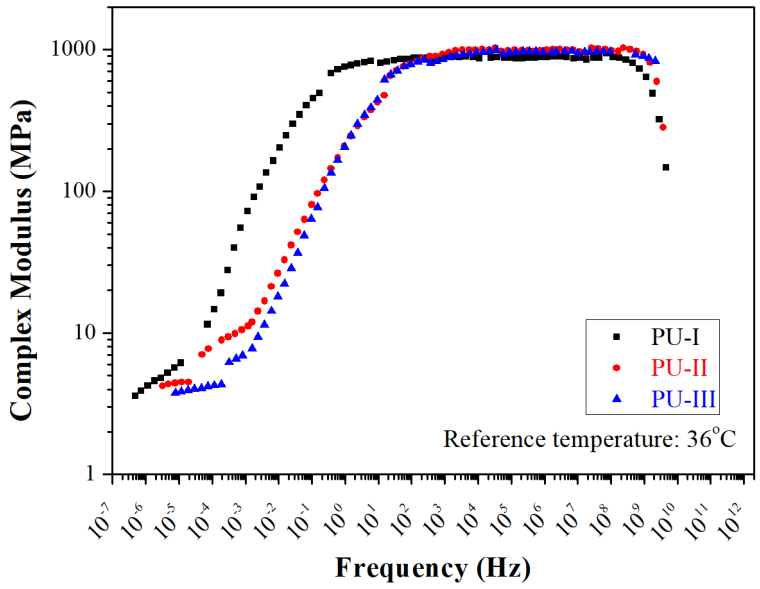

Fig. 12 Evolutions in complex modulus (G*) of the PU binders as a function of frequency

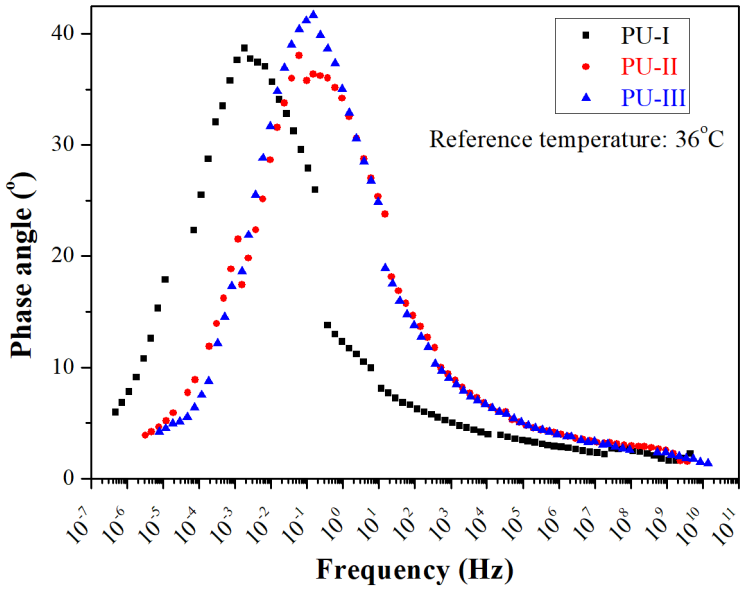

Fig. 13 Evolutions in phase angle of the PU binders as a function of frequency

As shown in Fig. 13, as the decrease in *R*, the phase angle decreases in the low-frequency region and increases slightly in the medium- and high-frequency regions at a fast rate and then a fairly slow rate. This result indicates that the viscosity-elasticity rate of the PU binder decreases and increases as the decrease in *R* in the low-frequency and high-frequency region, namely high-temperature and low-high-temperature region, respectively. Like the changes in the complex modulus, the phase angle also exhibited less obvious in the low *R*-value range. Therefore, combined with the changes of the complex modulus, the moderate increase in *R* can greatly improve the high-temperature performance of the PU mixture without significantly reducing its low-temperature.

5.2 Mechanical properties of PUMs

5.2.1 Marshall stability

The effects of *R* on both Marshall stabilities of the two PUMs before and after water immersion were investigated and their results are plotted in Fig. 14. As shown, both the Marshall stabilities of the two PUMs before and after water immersion increases with increasing *R*. This result indicates that the increase in *R* can enhance the interfacial bonding between PU and aggregates to a certain extent. For both the two PUMs after water immersion, the loss ratio of the Marshall stability exhibits relatively low values (~16.9% to ~21.2%) at the highest *R* while it increases to more than twice the value at low *Rs*, especially for the PU-II mixtures. Therefore, the PUMs with high *R* possess a better water stability resistance due to its good interfacial bonding

between PU and aggregates. It is noted that the PU-II mixtures show a higher loss ratio in the Marshall stability than the PU-III mixtures, which is believed to be caused by the mismatching between the large reduction in the initial value of the Marshall stability and degradation in Marshall stability after water immersion.

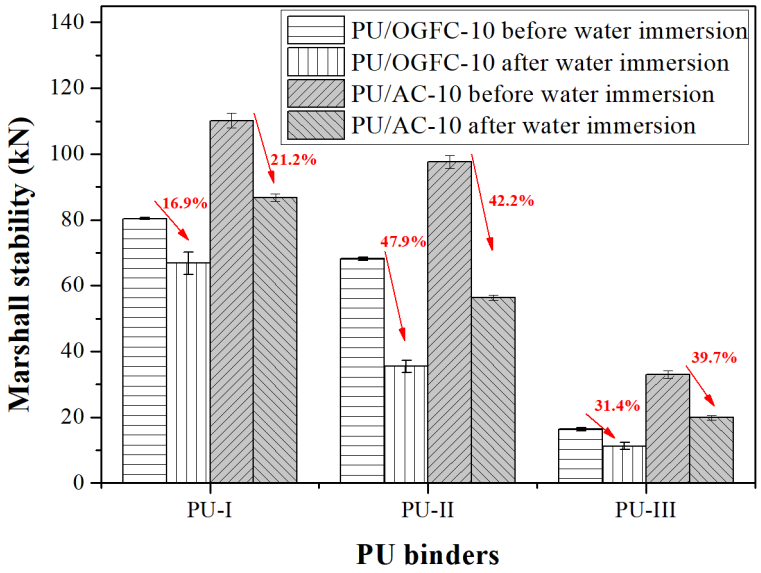

Fig. 14 The Marshall stability of both PU/OGFC-10 and PU/AC-10 mixtures with different *R*s

In contrast to the PU/OGFC-10 mixtures, the PU/AC-10 mixtures possess a significantly higher Marshall stability due to its denser gradation. After water immersion, both PU-I/AC-10 and PU-III/AC-10 mixtures show a slightly higher loss ratio in Marshall stability while the PU-II/AC-10 mixtures exhibit a lower Marshall stability than the PU/OGFC-10 mixtures. This result can be concluded that there is no obvious inherent law between the gradation and loss ratio in Marshall stability under different *R*s.

To further reveal the mechanism in the effects of *R* on the performance of the two PU mixtures, the FT-IR spectra of the PU binders were conducted and are plotted in Fig. 15. As shown, the peak at 2275.7 cm^{-1} is assigned as the unreacted −N=C=O groups, suggesting that some unreacted −N=C=O groups existed in the PU binders even with the lowest *R*. As the decrease of *R*, the height of the peak at 2275.7 cm^{-1} decreased significantly, in other words, the ratio of the unreacted −N=C=O groups increases with increasing *R*. After immersion, the uncreated −N=C=O groups can react with water molecule and produce ureido and carbon dioxide (seeing in Eq. (5)), which increases the chemical crosslinking of PU and further inhibits the degradation of the water resistance of Marshall stability to some extent. It should be noted that the above chemical reaction did not change the void ratio of PU mixture since it is a microscopic change and there are

only quite a few residual -NCO groups.

$$2R-N=C=O+H_2O \rightarrow R-NH-CO-NH-R+CO_2\uparrow \quad (5)$$

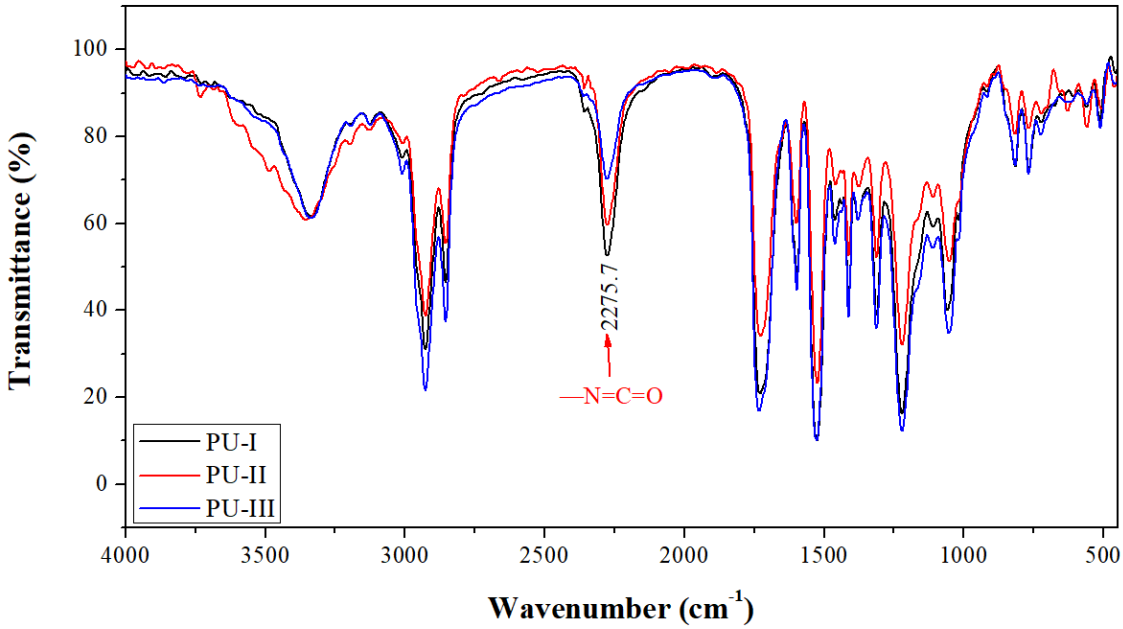

Fig. 15 The FT-IR spectra of the PU binders with different *R*s

5.2.2 Splitting strength

The effects of *R* on the splitting strength of two PUMs before and after freeze thawing are plotted in Fig. 16. As shown, similar with Marshall stability, the splitting strength of both two PUMs before and after freeze thawing increases significantly with increasing *R*, which also indicates that the increase in *R* can improve the interfacial bond between PU and aggregates and further enhance the splitting resistance of PUMs. After freeze-thawing, the ranges of degradation rate in splitting strength of PU/OGFC-10 and PU/AC-10 are 39.5%~66.4% and 48.8%~56.8%, respectively. Furthermore, the degradation rate increases with increasing *R*. Therefore, the freeze thawing has a considerable degradation effect on the splitting strength of PUMs due to its frost action.

Contrary to water intrusion, the increase in *R* can accelerate the degradation of mechanical properties for PUMs, which may be ascribed to the reduction in ductility. In other words, the increase in ductility of PU binders can help to improve the freeze-thaw resistance of PUM. In addition, in contrast to PU/OGFC-10, PU/AC-10 has higher degradation in splitting strength after freeze thawing, which is also related to its denser gradation. Combined with the results in Fig. 14, PU/OGFC-10 has a better water resistance than PU/AC-10.

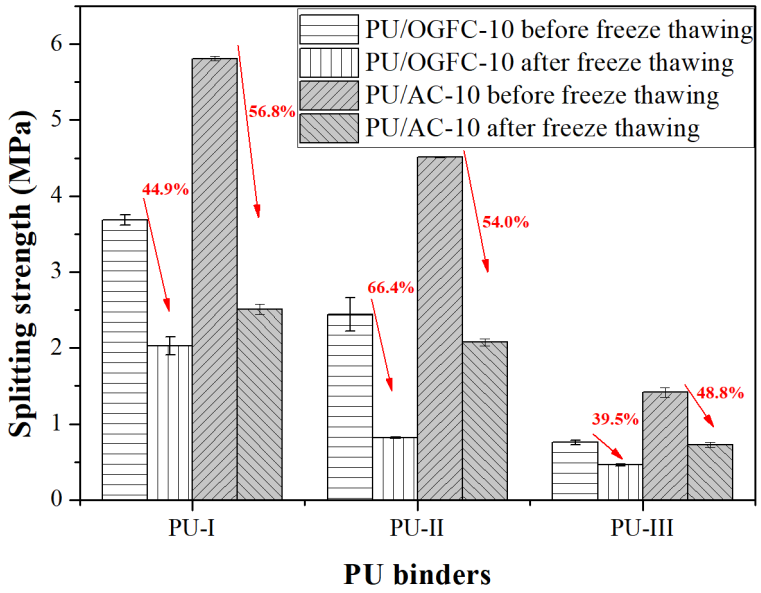

Fig. 16 The splitting strength of both OGFC-10 and AC-10 mixtures with different *R*s

5.2.3 Trabecular bending

As stated above, the increase in *R* has improved significantly the mechanical properties of PU mixtures. Therefore, only the trabecular bending properties of the two PU-I mixtures were conducted and plotted in Fig. 17. As can be seen from the corresponding data listed in Table 4, in contrast to PU-I/OGFC-10, PU-I/AC-10 has almost twice flexural strength and stiffness modulus, but only slightly lower flexural strain at both yield point and break point, which is also due to its denser gradation.

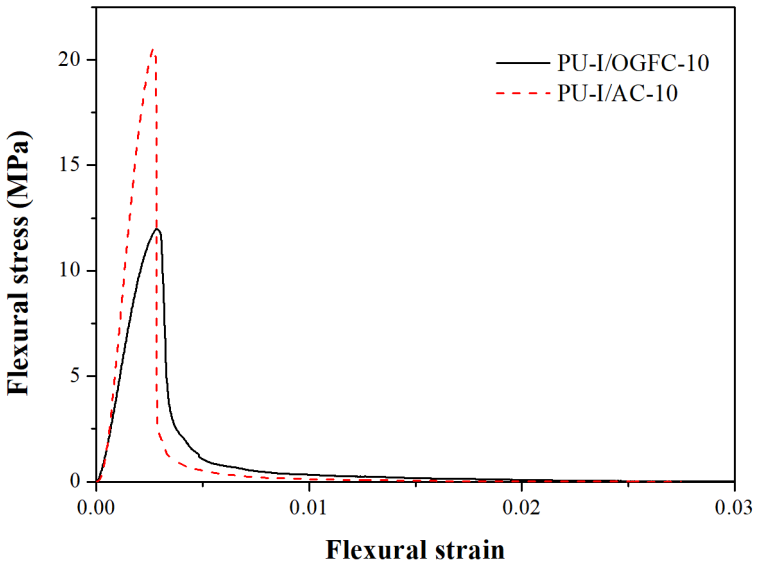

Fig. 17 The flexural stress-strain curves of both PU-I/OGFC-10 and PU-I/AC-10 mixtures

Table 4 Trabecular bending properties of two PU-I mixtures

PUMs	Flexural strength (MPa)	Maximum flexural strain (με)	Flexural stiffness modulus (MPa)
PU-I/OGFC-10	11.5 ± 0.8	2813.0 ± 386.7	4148.0 ± 674.4
PU-I/AC-10	20.6 ± 1.6	2664.4 ± 123.2	7735.8 ± 541.3

5.3 Functional properties of PUMs

5.3.1 Skid resistance

Based on the polishing simulation using HPM for 300 min, the MPD values and BPN values of AC-10, OGFC-10, PU/AC-10, and PU/OGFC-10 were obtained in Fig. 18. The power fitting method was applied to estimate the development of both MPD and BPN values in terms of polishing during (based on higher than 9.5 coefficient of determination).

As can be seen from Fig. 18a, it is found that the MPD of both PU/AC-10 and PU/OGFC-10 decreases continuously with time until it reaches a stable value, which is the same as the MPD development in the polishing test of asphalt mixtures. This shows that the texture depth is continuously decreasing, mainly because the coarse aggregates in the mixture are continuously polished, and the textures of the pavement surface are constantly smoothed. However, in detail, the MPD values of both PU/OGFC-10 and PU/AC-10 are higher than that of OGFC-10 and AC-10 throughout the early decay cycle. It can be known that the texture decay rate of PUM is lower than that of asphalt mixture, which is mainly attributed to the excellent abrasive resistance (Ashrafizadeh et al., 2016) and adhesion property (Cong et al., 2018) of the PU binder.

asphalt mixture surface properties will be significantly influenced by fatigue, moisture damage and long-term traffic loading, while PUM shows high resistance to those common problems.

The Fig. 18b shows the development of BPN during polishing, which is similar to that of MPD. BPN values of all samples increased with polishing time and then decreased slowly and continuously until it reached a stable value. The reason is that the PU binder is wrapped on the surface of the aggregate in the initial stage of the test samples. In a relatively short period of polishing time, the binder material is gradually polished, and then the aggregate is exposed. In this case, the skid resistance of PUM will increase in the

initial polishing stage. When the aggregate is fully exposed on the surface, the tire drives the polishing medium quartz sand and water to continuously produce polishing effects on the aggregate. Hence, the skid resistance of mixtures is continuously reduced by the aggregate is being continuously polished.

The initial BPN value of OGFC-10 is therefore higher than that of AC-10. However, the BPN value of PU/OGFC-10 was higher than AC-10 and OGFC-10 during the later polishing duration. The BPN value of PU/AC-10 was also higher than that of AC-10, and even higher than that of OGFC-10 for almost half of the total polishing time. It shows that the durability of the skid resistance of PU mixture pavement is higher than that of asphalt mixture pavement. It also implies that, by using the PU binder in tunnel pavement, the maintenance times and energy consumption can be saved to a certain extent.

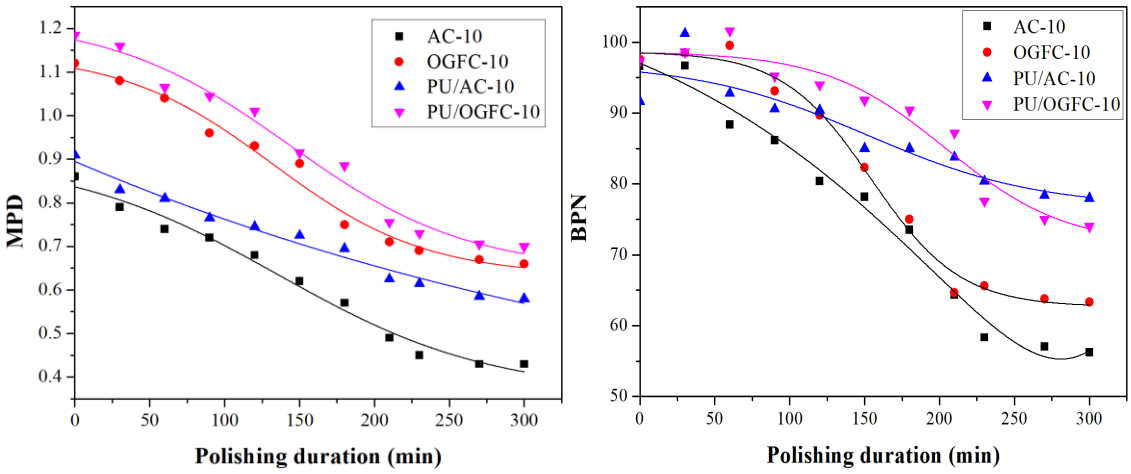

(a) (b)

Fig. 18 The evaluation of skid resistance based on HPM: (a) MPD test values; (b) BPN test values

5.3.2 Acoustic performance

The measured incident and reflected sound energy is used to calculate the sound absorption coefficient as a function of the frequency. With the impedance tube used here, the frequency range from 200 to 2000 Hz is covered, whereby the respective sound absorption coefficient is determined in steps of 3 Hz. Since this is a test method in which the specimens are not altered or damaged, each specimen is examined a total of three times, the averages are given in Fig. 19.

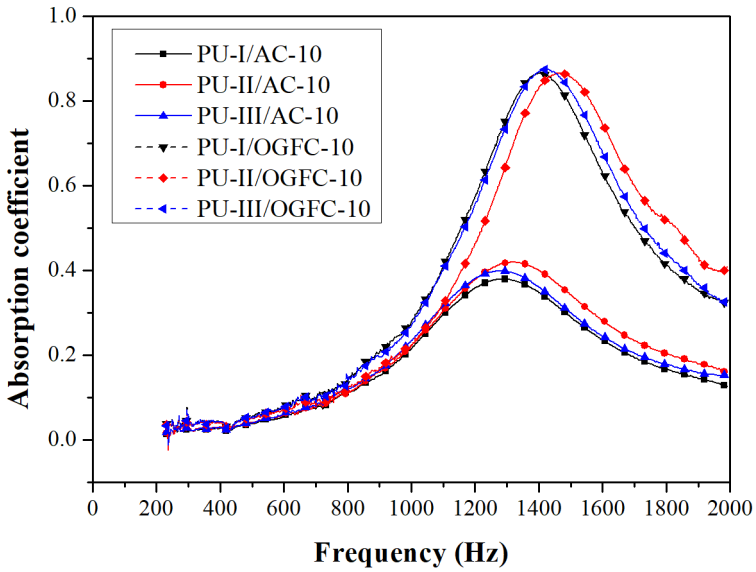

Fig. 19 Noise absorption coefficient measurements in accordance with ISO 10534-2.

It shows the absorption coefficients of the PU/OGFC samples in comparison to PU/AC. It can be seen that the absorption coefficients of the PU/OGFC samples are within the range of 30% to 85% between 1000 Hz and 2000 Hz, which is the important frequency range to human auditory perception (Lu et al., 2019a). From 200 Hz to 2000 Hz, PU/OGFC shows maximum absorption coefficients of 86%, at 1425 Hz. When comparing the results to PU/AC samples, the maximum absorption coefficients of PU/AC are much smaller than those of PU/OGFC (with a maximum 43% absorption coefficient at roughly 1270Hz). From the previous study, it is more important to compare the course of the absorption coefficient over the frequency than the absolute maximum absorption value. It can be seen that the PU/OGFC samples exhibit wider frequency ranges with high absorption coefficients in comparison to the PU/AC, which is an indicator of better noise absorption. In addition, the *R* of PU binders has few effects on the noise absorption in terms of PUMs.

5.3.3 Flammability evaluation

As a significant parameter for flammability evaluation of materials, the ignition time (TTI) is the time from heating the surface of materials to continuous combustion at a preset incident heat flux and can be used to evaluate the refractory properties of materials. TTIs of both PU/OGFC and PU/AC are plotted in Fig. 20, compared with OGFC and AC, respectively. As shown, TTI for PU/OGFC decreases slightly while TTI for PU/OGFC decreases firstly and then increases with decreasing *R*. However, the differences between different *R*s of PU binders are very small, which indicates that the *R* of PU binders has few effects on the TTI of PUMs, especially for PU/OGFC. The mean TTIs of PU/OGFC and PU/AC are 292.0 $\pm$ 6.2 s and 301.7 $\pm$ 17.1

s, respectively. Hence, PU/AC has a better combustion resistance, which is similar with asphalt-based mixtures. In contrast to asphalt-based mixtures, TTIs of PU/OGFC and PU/AC are 3.3 and 2.1 times of that of OGFC and AC, respectively. This result shows that PUMs have excellent combustion resistance far better than asphalt mixtures.

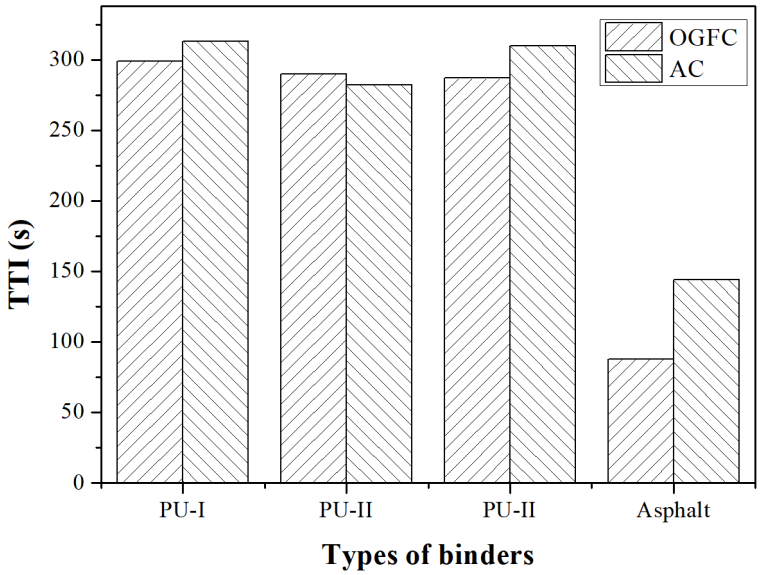

Fig. 20 TTIs between PU- and asphalt-based mixtures

The other two important parameters representing flame retardation are heat release rate (HRR) and total heat release (THR) from ignition to flame extinction, respectively. The peak value of HRR is designed as pkHRR. HRRs and THRs of both PU/OGFC and PU/AC are plotted in Fig. 21 and Fig. 22, compared with OGFC and AC, respectively.

As shown in Fig. 21, all the HRR at the same time, burning duration, pkHRR and THR increases slightly with increasing *R* for both PU/OGFC and PU/AC, especially for PU/OGFC, implying that the increase of *R* can enhance the risk of combustion. In contrast to PU/OGFC, PU/AC has a little higher pkHRR and THR due to its more aggregates. In addition, it is noted that asphalt-based mixtures, compared to PUMs, has significantly higher pkHRR, shorter burning duration and lower THR, which indicates that the asphalt-based mixtures have a fairly high heat release rate and can burn very quickly. Therefore, it can be concluded that the asphalt-based mixtures are more dangerous than PUMs in case of fire, and PUMs can greatly reduce the risk of combustion.

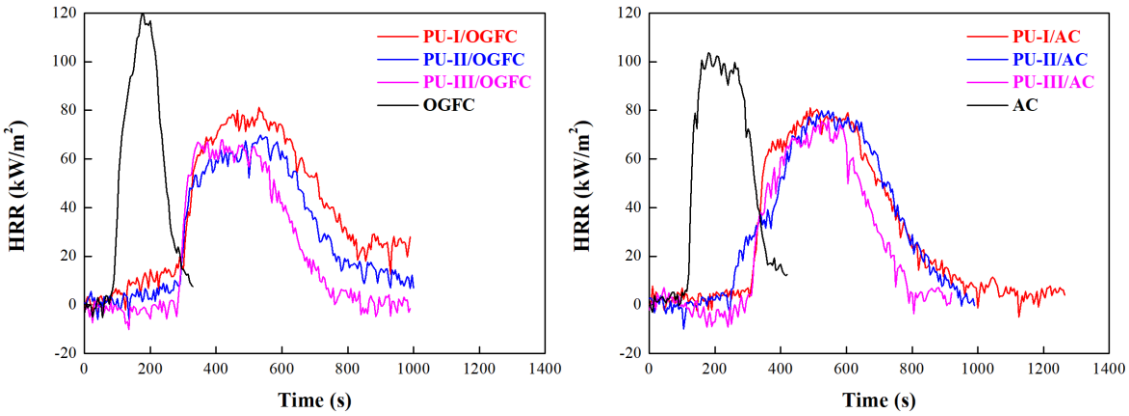

(a) (b)

Fig. 21 HRRs between PU- and asphalt-based mixtures. (a) OGFC, (b) AC

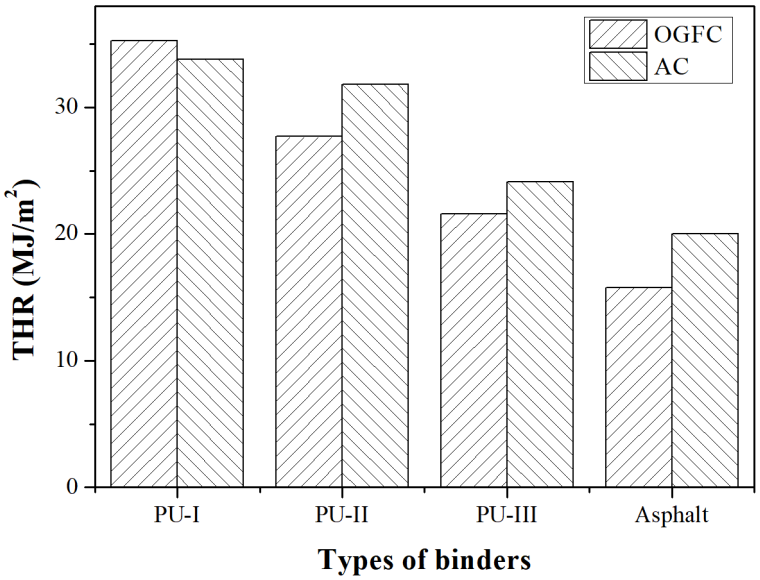

Fig. 22. THRs between PU- and asphalt-based mixtures

6 Conclusions

In the present research, a new polyurethane (PU) ultra-thin friction course with both low environmental impact and excellent pavement properties used in the tunnel, was proposed. The environmental impact evaluation, mechanical properties and functional properties of PUM were investigated systematically. The detailed conclusions are as follows:

1) Contrary to asphalt mixtures, due to the room temperature construction condition, polyurethane mixtures (PUMs) have low global warming potential (GWP) and energy consumption, exhibiting superior

environmental benefits for tunnel pavement.

2) Both PU/OGFC and PU/AC have excellent mechanical properties, which can be significantly enhanced by the isocyanate index (*R*), due to its outstanding interfacial bonding between PU and aggregates. However, PUM has relatively poor water stability due to its less ductility of PU according to the water immersion test and freeze-thawing test. In contrast to PU/OGFC, PU/AC possesses higher mechanical properties but weaker water stability.

3) In general, PUM shows a better skid resistance comparing to the asphalt mixtures. The PU/OGFC shows better skid resistance than PU/AC. Apart from it, PUM also possesses higher noise absorption performance, especially for PU/OGFC, which cannot be influenced obviously by *R*.

4) From the safety aspect of tunnel pavement, PUM has an excellent flame retardant performance, such as longer ignition time (TTI) and burning duration, lower heat release rate (HRR) but higher total heat release (THR), especially for PU/AC.

Given the mentioned excellent performance and poor water stability of PUM, future works may be proposed as follows: 1) Study the long-term service performance of PUM and improve its weaknesses, including the water stability; 2) Propose a kind of supporting construction technology of PUM; 3) Realize the intelligent monitoring function of PUM.

Acknowledgements

This work was financially supported by the National Key Research and Development Program of China (Grant No. 2018YFB1600100), China Postdoctoral Science Foundation funded project (Grant No. BX20180088), Heilongjiang Postdoctoral Fund (Grant No. LBH-Z18083) and Key Laboratory of Road and Traffic Engineering of Ministry of Education (Grant No. K201801), Tongji University. The authors are solely responsible for the content.

References

Ashrafizadeh, H., Mertiny, P., and McDonald, A., 2016. Evaluation of the effect of temperature on mechanical properties and wear resistance of polyurethane elastomers. Wear. 368, 26-38. http://doi.org/10.1016/j.wear.2016.08.008

552 Bonati, A., Merusi, F., Polacco, G., Filippi, S., and Giuliani, F., 2012. Ignitability and thermal
553 stability of asphalt binders and mastics for flexible pavements in highway tunnels.
554 Constr. Build. Mater. 37, 660-668. http://doi.org/10.1016/j.conbuildmat.2012.07.096
555 Cong, L., Wang, T.J., Tan, L., Yuan, J.J., and Shi, J.C., 2018. Laboratory evaluation on
556 performance of porous polyurethane mixtures and OGFC. Constr. Build. Mater. 169,
557 436-442. http://doi.org/10.1016/j.conbuildmat.2018.02.145
558 Harvey, J.T., Meijer, J., Ozer, H., Al-Qadi, I.L., Saboori, A., and Kendall, A., 2016. Pavement
559 Life Cycle Assessment Framework (No. FHWA-HIF-16-014). Federal Highway
560 Administration, United States. https://trid.trb.org/view/1420352
561 Hepburn, C., 1992. Polyurethane elastomers, Springer, Netherlands.
562 https://link.springer.com/book/10.1007/978-94-011-2924-4
563 Hong, B., and Xian, G., 2018. Ageing of a thermosetting polyurethane and its pultruded carbon
564 fiber plates subjected to seawater immersion. Constr. Build. Mater. 165, 514-522.
565 http://doi.org/10.1016/j.conbuildmat.2018.01.042
566 Hong, B., Xian, G., and Li, H., 2018. Effects of water or alkali solution immersion on the water
567 uptake and physicomechanical properties of polyurethane. Polym. Eng. Sci. 58, 2276-
568 2287. http://doi.org/10.1002/pen.24848
569 Huang, L.Z., Bohne, R.A., Bruland, A., Jakobsen, P.D., and Lohne, J., 2015. Life cycle
570 assessment of Norwegian road tunnel. Int J Life Cycle Ass. 20, 174-184.
571 http://doi.org/10.1007/s11367-014-0823-1
572 Karbhari, V.M., 2006. Dynamic mechanical analysis of the effect of water on E-glass-vinylester
573 composites. J Reinf Plast Comp. 25, 631-644.
574 http://doi.org/10.1177/0731684406058274
575 Leng, C., Lu, G.Y., Gao, J.L., Liu, P.F., Xie, X.G., and Wang, D.W., 2019. Sustainable Green
576 Pavement Using Bio-Based Polyurethane Binder in Tunnel. Materials. 12.
577 http://doi.org/10.3390/ma12121990
578 Li, T., Lu, G.Y., Wang, D.W., Hong, B., Tan, Y.Q., and Oeser, M., 2019. Key properties of
579 high-performance polyurethane bounded pervious mixture. China. J. Highw. Transp.
580 32, 162-173. http://zgglxb.chd.edu.cn/CN/article/searchArticleResultByKeyword.do#
581 Liu, P.F., Wang, D.W., Otto, F., Hu, J., and Oeser, M., 2018. Application of semi-analytical
582 finite element method to evaluate asphalt pavement bearing capacity. Int. J. Pavement.
583 Eng. 19, 479-488. http://doi.org/10.1080/10298436.2016.1175562
584 Lu, G.Y., Fan, Z.P., Sun, Z.Q., Liu, P.F., Leng, Z., Wang, D.W., and Oeser, M., 2020a.
585 Improving the polishing resistance of cement mortar by using recycled ceramic. Resour
586 Conserv Recy. 158. http://doi.org/10.1016/j.resconrec.2020.104796
587 Lu, G.Y., Liu, P.F., Torzs, T., Wang, D.W., Oeser, M., and Grabe, J., 2020b. Numerical analysis
588 for the influence of saturation on the base course of permeable pavement with a novel
589 polyurethane binder. Constr. Build. Mater. 240.
590 http://doi.org/10.1016/j.conbuildmat.2019.117930
591 Lu, G.Y., Liu, P.F., Wang, Y.H., Fassbender, S., Wang, D.W., and Oeser, M., 2019a.
592 Development of a sustainable pervious pavement material using recycled ceramic
593 aggregate and bio-based polyurethane binder. J. Clean. Prod. 220, 1052-1060.
594 http://doi.org/10.1016/j.jclepro.2019.02.184
595 Lu, G.Y., Renken, L., Li, T.S., Wang, D.W., Li, H., and Oeser, M., 2019b. Experimental study
596 on the polyurethane-bound pervious mixtures in the application of permeable
597 pavements. Constr. Build. Mater. 202, 838-850.
598 http://doi.org/10.1016/j.conbuildmat.2019.01.051
599 Lu, G.Y., Torzs, T., Liu, P.F., Zhang, Z.Y., Wang, D.W., Oeser, M., and Grabe, J., 2020c.
600 Dynamic Response of Fully Permeable Pavements: Development of Pore Pressures

under Different Modes of Loading. J. Mater. Civ. Eng. 32. http://doi.org/10.1061/(Asce)Mt.1943-5533.0003217

Lu, G.Y., Wang, Z.J., Liu, P.F., Wang, D.W., and Oeser, M., 2020d. Investigation of the Hydraulic Properties of Pervious Pavement Mixtures: Characterization of Darcy and Non-Darcy Flow Based on Pore Microstructures. J Transp Eng B-Pave. 146. http://doi.org/10.1061/Jpeodx.0000161

Moretti, L., Cantisani, G., and Di Mascio, P., 2016. Management of road tunnels: Construction, maintenance and lighting costs. Tunn Undergr Sp Tech. 51, 84-89. http://doi.org/10.1016/j.tust.2015.10.027

Norman, J., MacLean, H.L., and Kennedy, C.A., 2006. Comparing high and low residential density: Life-cycle analysis of energy use and greenhouse gas emissions. J Urban Plan D-Asce. 132, 10-21. http://doi.org/10.1061/(Asce)0733-9488(2006)132:1(10)

Qiu, J.L., Yang, T., Wang, X.L., Wang, L.X., and Zhang, G.L., 2019. Review of the flame retardancy on highway tunnel asphalt pavement. Constr. Build. Mater. 195, 468-482. http://doi.org/10.1016/j.conbuildmat.2018.11.034

Qun, Y., and Guo, Z.Y., 2005. Mixture design of fire-retarded OGFC in road tunnel. Road Mater Pavement. 6, 255-268. http://doi.org/10.1080/14680629.2005.9690008

Santero, N.J., Masanet, E., and Horvath, A., 2011. Life-cycle assessment of pavements. Part I: Critical review. Resour Conserv Recy. 55, 801-809. http://doi.org/10.1016/j.resconrec.2011.03.010

Sun, Z.Q., Lin, X.C., Liu, P.F., Wang, D.W., Vollpracht, A., and Oeser, M., 2018. Study of alkali activated slag as alternative pavement binder. Constr. Build. Mater. 186, 626-634. http://doi.org/10.1016/j.conbuildmat.2018.07.154

Ueckermann, A., Wang, D.W., Oeser, M., and Steinauer, B., 2015. Calculation of skid resistance from texture measurements. J Traffic Transp Eng. 2, 3-16. http://doi.org/10.1016/j.jtte.2015.01.001

Wang, D.W., Liu, P.F., Leng, Z., Leng, C., Lu, G.Y., Buch, M., and Oeser, M., 2017a. Suitability of PoroElastic Road Surface (PERS) for urban roads in cold regions: Mechanical and functional performance assessment. J. Clean. Prod. 165, 1340-1350. http://doi.org/10.1016/j.jclepro.2017.07.228

Wang, D.W., Schacht, A., Leng, Z., Leng, C., Kollmann, J., and Oeser, M., 2017b. Effects of material composition on mechanical and acoustic performance of poroelastic road surface (PERS). Constr. Build. Mater. 135, 352-360. http://doi.org/10.1016/j.conbuildmat.2016.12.207

Wang, D.W., Wang, H.N., Bu, Y., Schulze, C., and Oeser, M., 2015. Evaluation of aggregate resistance to wear with Micro-Deval test in combination with aggregate imaging techniques. Wear. 338, 288-296. http://doi.org/10.1016/j.wear.2015.07.002

Wang, H.P., Lu, G.Y., Feng, S.Y., Wen, X.B., and Yang, J., 2019. Characterization of Bitumen Modified with Pyrolytic Carbon Black from Scrap Tires. Sustainability-Basel. 11. http://doi.org/10.3390/su11061631

Yang, Q.L., Li, X.L., Zhang, L., Qian, Y., Qi, Y.Z., Kouhestani, H.S., Shi, X.M., Gui, X.C., Wang, D.W., and Zhong, J., 2020. Performance evaluation of bitumen with a homogeneous dispersion of carbon nanotubes. Carbon. 158, 465-471. http://doi.org/10.1016/j.carbon.2019.11.013

Zhang, H., Lepech, M.D., Keoleian, G.A., Qian, S.Z., and Li, V.C., 2010. Dynamic Life-Cycle Modeling of Pavement Overlay Systems: Capturing the Impacts of Users, Construction, and Roadway Deterioration. J Infrastruct Syst. 16, 299-309. http://doi.org/10.1061/(Asce)Is.1943-555x.0000017

649 Zhao, H., Li, H.P., and Liao, K.J., 2010. Study on Properties of Flame Retardant Asphalt for
650 Tunnel. Petrol Sci Technol. 28, 1096-1107. http://doi.org/10.1080/10916460802611465
651